Three-Dimensional Super-Wideband Micro-Antenna for High-Resolution Millimeter-Wave Medical Imaging

Amir Mirbeik, *Student Member, IEEE*, Vahid Tavassoli, *Member, IEEE*,
Farrokh Ayazi, *Fellow*, *IEEE,* and Negar Tavassolian, *Member, IEEE*

***Abstract*—This paper reports on a novel super-wideband micro-hemispherical antenna with application in millimeter-wave medical imaging. The antenna is composed of a hemispherical shell suspended above a substrate and can be fabricated using a fabrication technology originally developed for micron-scale electromechanical resonators. The antenna exhibits a wide fractional bandwidth of more than 80% (from 64 GHz to 150 GHz) and a high gain of 8.6 dBi at its center frequency. Radiation parameters of the antenna are characterized and the effect of its super-wideband behavior on pulsed millimeter-wave imaging is demonstrated. Finally, a preliminary array configuration composed of two antennas placed side-by-side in the vicinity of a skin-mimicking target is evaluated and the ability to fully detect the target has been demonstrated.**

I. Introduction

Historically, devices operating in the millimeter-wave regime have been limited to specialized applications including wireless communications [1], radar [1], and imaging [2]. The unlicensed 60 GHz band is of interest for automotive and wireless applications [3]. However, there hasn't been enough effort to employ this available technology for use in medical systems. One particularly interesting application is the early detection of skin anomalies (e.g. skin cancer) by monitoring the skin in a non-invasive and harmless manner. Compared to X-ray imaging which utilizes ionizing radiation and may lead to malignancies, microwave and millimeter-wave radiations are non-ionizing and consequently harmless [4].

Microwave radiation has the potential to effectively discriminate between healthy and cancerous tissues and has been employed in various prototypes to produce medical images [5-8]. This band involves relatively lower frequencies, which guarantees significant penetration of the electromagnetic waves in the human tissue. Whereas microwave imaging systems are simpler due to their low operation frequencies, they are bulky and inconvenient for system-level integration. Furthermore, they lack the high spatial resolutions required for certain applications such as skin cancer diagnosis. In comparison to microwave radiation, millimeter waves benefit higher resolutions as well as sufficient penetration into the skin. As we further move to higher operation frequencies (i.e. the THz regime), electromagnetic waves have almost no penetration in the tissue [9].

The dielectric permittivity of the skin is directly proportional to its water content in the millimeter-wave regime [10]. Since the water content of cancerous tissues is significantly higher than their normal healthy counterparts [11], millimeter waves can provide high dielectric contrasts between cancerous and normal tissues. These advantages lead the millimeter-wave band to be of great interest for medical imaging.

Millimeter-wave imaging can be performed using different approaches, ranging from single-frequency operations to wideband (pulsed) imaging methodologies [2]. A pulsed millimeter-wave imaging system for biomedical applications has already been introduced [12]. This system operates at a center frequency of 30 GHz with a bandwidth of 20 GHz and provides a high range resolution (defined as the minimum detectable feature size in the direction of the transmitting wave).

In wideband pulsed-imaging applications, the range resolution is given by [2]:

$$\delta_z \approx \frac{c}{2B}, \qquad (1)$$

where B is the bandwidth of the system and c is the speed of light in the transmitting medium. Thus, a high range resolution pulsed-imaging system requires a broadband antenna as its central element.

In this paper, a novel three-dimensional super-wideband miniaturized antenna, namely the Micro-Hemispherical Shell Antenna (μ-HSA), is introduced for the first time. The antenna benefits from several key characteristics which make it a prime candidate for use in millimeter-wave imaging systems. These characteristics are as follows: 1) an extremely wide input impedance bandwidth (~80%) from 64 GHz to 150 GHz centered at 106 GHz, which provide for high lateral and range resolutions (due to the antenna's high operation frequency and super-wideband behavior, respectively), 2) a three-dimensional fully-symmetric structure which guarantees a symmetrical gain pattern for balanced and symmetrical scanning of the skin, and 3) a novel three-dimensional micro-fabrication platform which allows for antenna integration in the frontend and consequent development of a compact, highly-integrated system. This is fundamental in developing a cost-effective imaging system aimed at widespread use in population screening.

A. Mirbeik and N. Tavassolian are with the Department of Electrical and Computer Engineering, Stevens Institute of Technology, Hoboken, NJ 07030 (amirbeik@stevens.edu, negar.tavassolian@stevens.edu).

V. Tavassoli and F. Ayazi are with the School of Electrical and Computer Engineering, Georgia Institute of Technology, Atlanta, GA 30308 (vtavassoli3@mail.gatech.edu, ayazi@gatech.edu).

978-1-4244-7929-0/14/$26.00 ©2014 IEEE

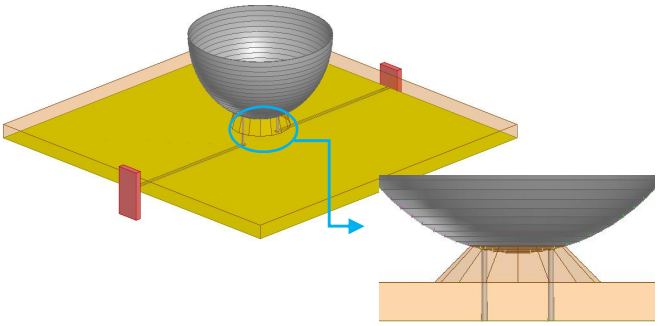

Figure 1. Geometry of the CWP-fed μ-HSA. The shell-antenna has a diameter of 1600 microns and is 5 microns thick.

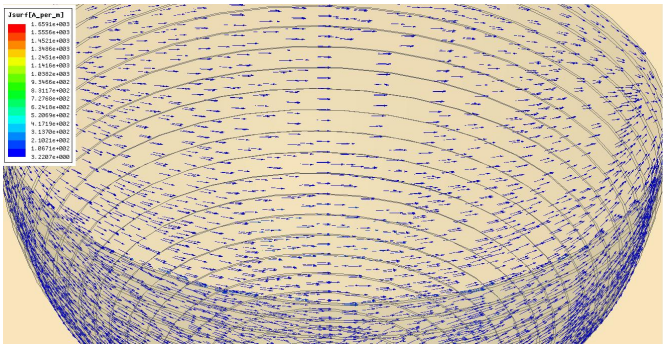

Figure 2. Surface current distribution on the μ-HSA at 106 GHz in the differential mode. The current lines rotate around the shell surface, yielding a directional radiation pattern.

The complete geometry of the antenna and its full characterization results are presented in section II. Section III evaluates the antenna performance in a wideband pulsed-imaging system, and Section IV concludes the paper and summarizes future directions.

II. Antenna Geometry and Characterization

The proposed antenna is composed of a hemispherical shell suspended above a high-resistivity Silicon substrate, and can be implemented using a micro-fabrication technology originally developed for three-dimensional resonators [13]. A representative 5-μm-thick, 1600-μm-diameter Micro-Hemispherical Shell Antenna supported on a thin (100-μm-diameter) stem is demonstrated in Fig. 1. The antenna is fed by two CPW lines which are electroplated on the Silicon substrate and are connected to the stem from opposite directions. The antenna can be operated in two separate modes, namely the common and differential modes. Both modes of the shell-antenna can be excited by this feeding configuration. When the lines exhibit 0° phase difference at the stem location (in-phase excitation), the common mode is excited. In this case, the radiation pattern of the antenna is omnidirectional. In contrast, the differential mode is excited when the two lines feed the shell with 180° phase difference (out-of-phase excitation), which forces the current lines to rotate around the shell surface (Fig. 2). The antenna demonstrates a high-gain performance in this mode, and is of interest for medical applications for efficient scanning of the imaging area. Antenna simulations are performed using ANSOFT HFSS [14], with copper assigned as the shell structural material.

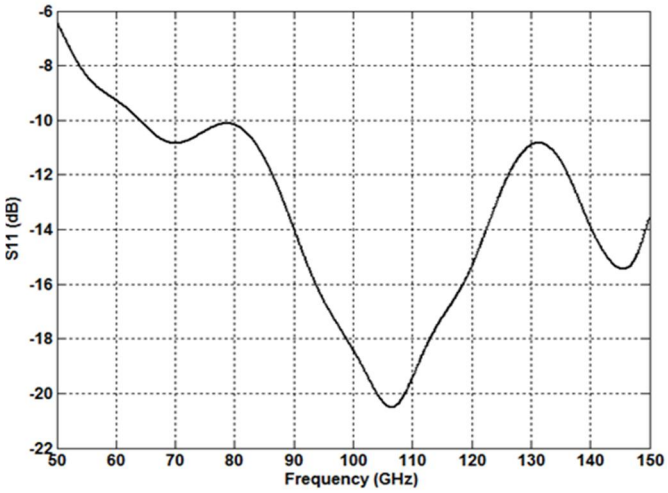

Figure 3. Return loss (S11) of the antenna for a feed line with a reference impedance of 50 Ω. A bandwidth of more than 86 GHz (from 64 GHz to >150 GHz) has been achieved.

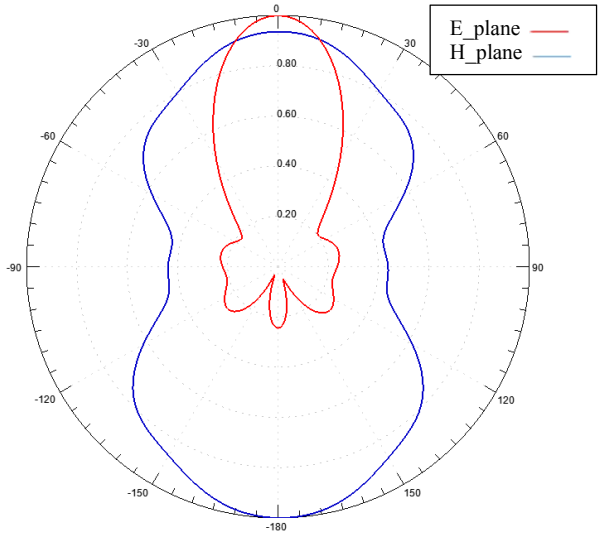

Figure 4. Normalized radiation pattern at 106 GHz, showing the highly-directive characteristic of the antenna in the differential mode.

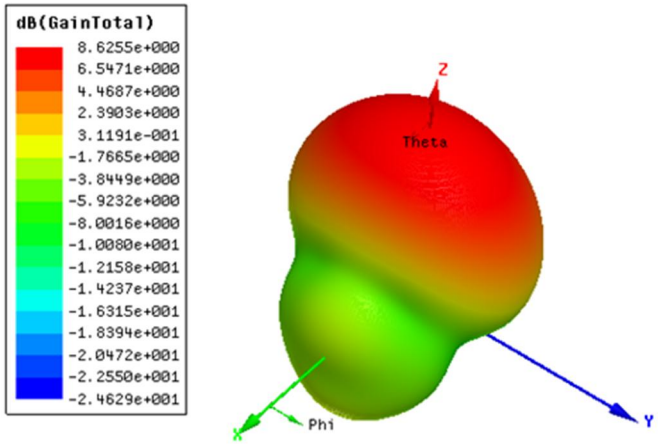

Figure 5. Three-dimensional gain pattern of the antenna at 106 GHz. A high gain value of 8.62 dBi is achieved.

TABLE I. RADATION PARAMETERS OF THE ANTENNA

BW%	80%
Radiation Efficiency at 106 GHz	69%
Gain (dBi) at 106 GHz	8.62
Directivity (dBi) at 106 GHz	10.25

Fig. 3 presents the antenna S11 in the 50-150 GHz range. The antenna demonstrates more than 86 GHz bandwidth from 64 GHz to >150 GHz. The normalized radiation pattern and the gain of the antenna are shown in Fig. 4 and Fig. 5, respectively. Another important parameter for the characterization of any antenna is its radiation efficiency, which is calculated as 69% for the shell antenna at 106 GHz. Table 1 summarizes the radiation parameters of the antenna at the center frequency of 106 GHz.

III. ANTENNA PERFORMANCE IN PULSED IMAGING

As already mentioned, in pulsed millimeter-wave imaging systems a super-wideband pulse needs to be generated. Pulse simulations are generally performed in a time-domain solver, such as CST Microwave Studios [15]. However, since the shell antenna is excited differentially by two ports, pulse simulations are more conveniently carried out in a frequency solver (for example ANSYS HFSS). In this regard, we implemented an approach that exploits the S-parameters of an antenna system (as its transfer function) to deduce the pulse response in the frequency domain. The pulse response is then transferred to the time domain by applying an Inverse Fourier Transform (IFFT) operation. Another advantage of our method is that it will alleviate the complicated procedure of super-wideband pulse generation in future experiments.

A Gaussian pulse with 3-dB bandwidth of 86 GHz and central frequency of 106 GHz is considered as the input pulse to the antenna system.

$$v(t) = \sin[2\pi f_0(t - t_0)] \exp\left[-\frac{(t - t_0)}{2\tau^2}\right], \qquad (2)$$

where $f_0 = 107$ GHz, $\tau = 3$ ps, and $t_0 = 500$ ps.

A. *The Effect of the Super-Wideband Characteristic of the Antenna on Pulsed Imaging*

Antenna fidelity, defined as the peak of the cross-correlation function between the input (incident) and output pulses is employed as a relevant metric to evaluate its performance in a wideband pulsed millimeter-wave imaging system. Antenna fidelity indicates the resemblance between the incident and received pulses and is calculated as [16]:

$$F = \max_\tau \int_{-\infty}^{+\infty} \hat{r}(t - \tau).\hat{f}(t)dt, \qquad (3)$$

where $\hat{r}(t)$ is the normalized received electrical field and $\hat{f}(t)$ is the normalized time derivative of the input signal at the antenna terminal.

Since we perform fidelity simulations in the frequency domain, S-parameters need to be calculated. In this case, the antenna fidelity is obtained by simulating at least two antennas to obtain the S21 parameter. After multiplying the input pulse by the S21 of the two-antenna system in the spectrum domain, we apply an IFFT operation using a customized code which we developed in MATLAB and obtain the pulse response in time domain.

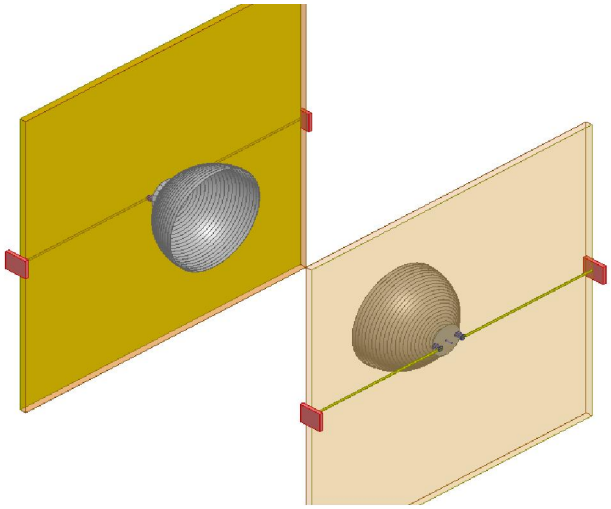

Figure 6. Antenna configuration when placed in front of each other with a distance of 5 mm. The fidelity is calculated as 82%.

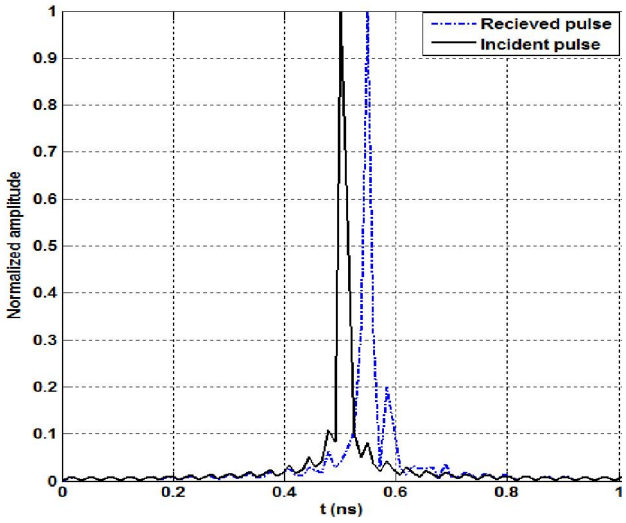

Figure 7. Normalized incident and received pulses for the case where the antennas are placed side-by-side (fidelity=96%).

Two antenna configurations are simulated for fidelity evaluations. The first configuration is shown in Fig. 6. The antennas are placed in front of each other, with a distance of 5 mm between the centers. This distance is typically used for fidelity evaluation of antennas [17]. A fidelity value of 82% is achieved in this case. The fidelity increases as the distance between the antennas is decreased [17]. In the second configuration (Fig. 8 without considering a target), the antennas are placed next to each other in the same plane. This is a more practical case in skin imaging methodologies. Both the incident pulse (original Gaussian pulse given as an input to the first antenna) and the received pulse (by the second antenna) are demonstrated in Fig. 7. A fidelity value of 96% is achieved when the distance between the antennas is 8 mm (estimated distance between two representative antennas in a skin imaging array). This fidelity is higher than what was achieved in the previous configuration (due to the reduction of mutual coupling between the antennas) and is also higher than what has been reported elsewhere [18].

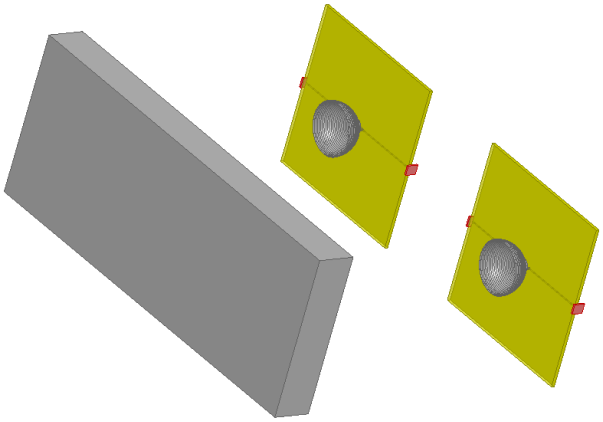

Figure 8. Antenna configuration for evaluation of the backscattered pulse response from a PEC cube.

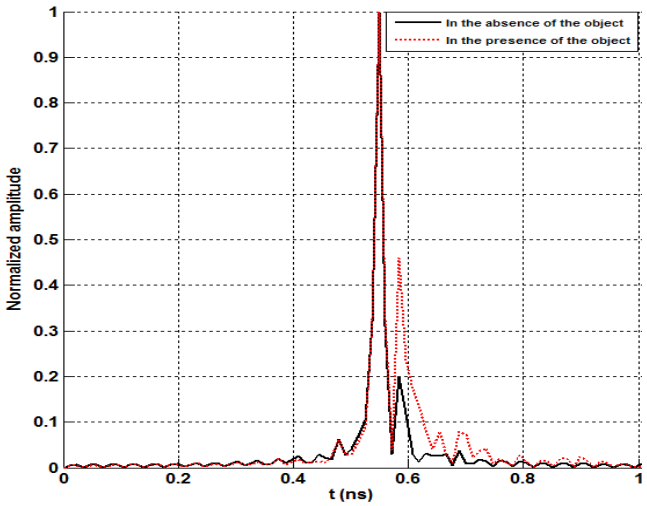

Figure 9. Normalized pulse responses in the presence and absence of the target. The presence of the target is fully observable.

B. Skin Tissue Response

In general pulsed-imaging systems, a narrow incident pulse is used to propagate into the imaging domain. An image is subsequently created from the backscattered pulse which contains the impact of target. To show the antenna performance in this context, two simulations are performed, one in the presence of a target and the other in its absence. As shown in Fig. 8, the target considered is a PEC rectangular cube mimicking the effect and geometry of the skin tissue. The size of the cube is realistically set as $13mm \times 5mm \times 1.2mm$. Two response pulses, one in the absence of the target (direct response) and the other in its presence (reflection from the target), are shown in Fig. 9. A significant difference is observed between these pulses, demonstrating the fact that the target is fully observable. Suitable metrics will be employed in the future to quantify the difference between the two pulses. A tumor model will also be included in the skin phantom.

IV. Conclusion

A novel super-wideband antenna for pulsed millimeter-wave imaging applications is proposed. The antenna can be built using a novel MEMS technology on a high-resistivity Silicon substrate. The antenna is characterized by a high gain (>8 dBi) and an extremely wide fractional bandwidth (~80%) at the central frequency of 106 GHz. The effect of the super-wideband characteristic of the antenna on pulsed millimeter-wave imaging applications is also demonstrated.

Our future work involves modifying the fabrication process of the resonators towards fabrication and characterization of the antenna. A wideband imaging algorithm will be employed to obtain an image from a representative target. The antenna will finally be employed in a suitable array configuration for medical imaging applications.

References

[1] R. M. Emrick and J. L. Volakis, "Antenna Requirements for Short Range High Speed Wireless Systems Operating at Millimeter-wave Frequencies," *IEEE IMS International Microwave Symposium*, San Francisco, CA, pp. 974–977, 2006.

[2] D. M. Sheen, D. L. McMakin, and T. E. Hall, "Three-Dimensional Millimeter-Wave Imaging for Concealed Weapon Detection," *IEEE Trans. Microw. Theory Tech.*, vol. 49, pp. 1581–1592, 2001.

[3] C. Doan, S. E. Mami, D. Sobel, A. Niknejad, and R. Brodersen, "60 GHz CMOS Radio for Gb/s Wireless LAN," *IEEE Radio Frequency Integrated Circuits Conference,* pp. 225–228, 2004.

[4] R. L. Brent "The Effect of Embryonic and Fetal Exposure to X-ray, Microwaves, and Ultrasound: Counseling the Pregnant and Nonpregnant Patient about These Risks," *Semin Oncol,* vol. 6, pp. 347-368, 1989.

[5] M. Pastorino, "Medical and Industrial Applications of Inverse Scattering Based Microwave Imaging Techniques," *IEEE Imaging Systems and Techniques,* 2008.

[6] P. Mojabi, J. LoVetri, and L. Shafai, "A Multiplicative Regularized Gauss–Newton Inversion for Shape and Location Reconstruction," *IEEE Trans. Antennas Propag.*, vol. 59, pp. 4790-4802, 2011.

[7] E. C. Fear, X. Li, S. C. Hagness, and M. Stuchly, "Confocal Microwave Imaging for Breast Cancer Detection: Localization of Tumors in Three Dimensions," *IEEE Trans. Biomed Eng.*, vol. 49, pp. 812–822, 2002.

[8] N. Tavassolian, S. Nikolaou, M. Tentzeris, "Microwave Tumor Detection Using a Flexible UWB Elliptical Slot Antenna with a Tuning Uneven U-shape Stub on LCP," *Proc. IEEE Antennas and Propagation Society International Symposium*, pp. 257-260, 2007.

[9] C. S. Joseph, A. N. Yaroslavsky, V. A. Neel, T. M. Goyette, and R. H. Giles, "Continuous Wave Terahertz Transmission Imaging of Nonmelanoma Skin Cancers," *Lasers in Surgery and Medicine*, vol. 43, pp. 457-462, 2011.

[10] S. Alekseev and M. Ziskin, "Human Skin Permittivity Determined by Millimeter Wave Reflection Measurements," *Bioelectromagnetics*, vol. 28, pp. 331–339, 2007.

[11] R. Pethig "Dielectric Properties of Biological Materials: Biophysical and Medical Applications," *IEEE Trans Elect Insulation*, vol. E1-19, pp. 453–474, 1984.

[12] S. Moscato, G. Matrone, M. Pasian, A. Mazzanti, M. Bozzi, L. Perregrini, F. Svelto, G. Magenes, P. Arcioni, and P. Summers, "A Mm-Wave 2D Ultra-Wideband Imaging Radar for Breast Cancer Detection," *International Journal of Antennas and Propagation*, 2013.

[13] N. Mehanathan, P. Shao, V. Tavassoli, L. D. Sorenson, and F. Ayazi, "Invar-36 Microhemispherical Shell Resonators," *IEEE MEMS,* pp. 40-43, 2014.

[14] http://www.ansoft.com/products/hf/hfss

[15] https://www.cst.com/

[16] X. Li, S. C. Hagness, M. K. Choi, and D. W. Van derWeide, "Numerical and Experimental Investigation of an Ultrawideband Ridged Pyramidal Horn Antenna with Curved Launching Plane for Pulse Radiation," *IEEE Antennas Wireless Propag. Lett.*, vol. 2, pp. 259–262, 2003.

[17] H. M. Jafari, M. Jamal Deen, S. Hranilovic, and N. K. Nikolova, "A Study of Ultrawideband Antennas for Near-Field Imaging," *IEEE Trans. Antennas Propag.*, vol. 55, pp. 1184-1188, 2007.

[18] H. Kanj and M. Popovic, "Miniaturized Microstrip-Fed "Dark Eyes" Antenna for Near-Field Microwave Sensing," *IEEE Antennas and Wireless Propagation Letters*, vol. 4, pp. 397-401, 2005.